NUCL SCI TECH (2022) 33:42
https://doi.org/10.1007/s41365-022-01026-w

Dication-accelerated anion transport inside micropores for the rapid decontamination of pertechnetate

Peng Zhang[1] · Yi-Zhi Chen[1] · Han-Qin Weng[1,2] · Zi-Fang Guo[1] · Jia-Liang Chen[1] · Xing Zhao[1] · Guo-An Ye[3] · Ming-Zhang Lin[1]

Received: 16 November 2021 / Revised: 11 February 2022 / Accepted: 12 March 2022 / Published online: 19 April 2022

Abstract Over 70% of the treated contaminated water at the Fukushima Daiichi Nuclear Power Station contains radionuclides beyond the regulatory standard for discharge that need to be re-purified. Technetium-99 (^{99}Tc), mainly in the form of pertechnetate Tc(VII)O_4^-, is one of the main sources of long-term radiotoxicity that jeopardizes the environment and human health. Herein, we used a series of dicationic pyridinium (DCP) derivative groups (–$Py^+C_nH_{2n}N^+Me_3$, n = 2, 3, and 5) to modify commercial Reillex 425 resins containing tertiary pyridyl groups to improve the adsorption performance of rhenium (Re, an analog of radioactive Tc) and Tc. As the quaternary pyridinium and ammonium sites in one DCP group can adsorb ReO_4^- simultaneously, DCP-modified Reillex 425 (Reillex-Cn) exhibited high maximum adsorption capacities for Re under neutral conditions. Adsorption capacities reached 344.8, 416.7, and 588.2 mg g^{-1} for Reillex 425-C2, Reillex 425-C3, and Reillex 425-C5, respectively. Intraparticle diffusion of ReO_4^-/TcO_4^- in Reillex 425-Cn was verified to be the rate-limiting step of adsorption. However, adsorption can be adjusted by the length of the alkyl spacers between the two positively charged N sites in DCP. –$Py^+C_2H_4N^+Me_3$ significantly enhanced intraparticle diffusion compared to –$Py^+C_5H_{10}N^+Me_3$. The two positive sites in –$Py^+C_2H_4N^+Me_3$ would be laterally distributed, leading to a smaller steric hindrance for ReO_4^-/TcO_4^- transport inside the microporous channels. Meanwhile, the longer alkyl spacers in –$Py^+C_5H_{10}N^+Me_3$ formed hydrophobic microphases, repulsing the hydrated ReO_4^-/TcO_4^- anions. Thus, the adsorptions of both ReO_4^- and TcO_4^- on Reillex 425-C2 were faster than those on Reillex 425-C5. Moreover, Reillex 425-Cn exhibited an exothermic nature, good selectivity, excellent reusability, and strong salinity tolerance. This study provides a simple strategy to enhance the Tc removal performance of adsorbents containing abundant micropores, which implies enormous environmental and economic benefits.

Keywords Quaternary pyridinium · Dicationic pyridyl derivatives · Pertechnetate · Intraparticle diffusion

1 Introduction

Approximately 6.3–7.7 × 10^{17} Bq of radioisotopes was released in the Fukushima nuclear accident (Level 7 event) [1, 2], among which technetium-99 (^{99}Tc) is one of the main sources of long-term radiotoxicity due to its long half-life of 2.13 × 10^5 years [3]. Tc mainly exists as soluble Tc(VII)O_4^- anions over a wide pH range and has the same configuration as sulfate (SO_4^{2-}) [4–6]. Thus, plants easily take up Tc in water, leading to its accumulation in animals. To date, treated contaminated water stored at the

---

This work was supported by the National Natural Science Foundation of China (Nos. 51803205, 11775214, and 21790371) and China Scholarship Council (No. 201906345006).

✉ Han-Qin Weng
hanqinw@ustc.edu.cn

[1] School of Nuclear Science and Technology, University of Science and Technology of China, Hefei 230026, China

[2] Department of Beam Material Science, SANKEN, The Institute of Scientific and Industrial Research, Osaka University, 8-1 Mihogaoka, Ibaraki, Osaka 567-0047, Japan

[3] Radiochemistry Department of China Institute of Atomic Energy, China Institute of Atomic Energy, Beijing 102413, China

Fukushima Daiichi Nuclear Power Station has reached 92% of the total capacity, 71% of which (over 0.9 million tons) does not meet the regulatory standard for discharge [7]. Re-purification to remove Tc before discharge is necessary to alleviate concerns regarding non-tritium radioactive isotopes that induce Tc [8].

As all Tc isotopes are radioactive, non-radioactive rhenium (Re) with chemical properties similar to those of Tc is usually used as an analog [9, 10]. Among the diverse methods developed for TcO_4^- (ReO_4^-) removal, including adsorption [11–13], solvent extraction [14], and reduction to oxide precipitates [15, 16], adsorption remains the most practical approach for treating a large volume of water with low contaminant concentrations [17]. After the Fukushima nuclear accident, the Tokyo Electric Power Company employed a comprehensive apparatus utilizing different adsorbents for seawater decontamination. Cetyltrimethylammonium-modified zeolites were used to remove TcO_4^- and other organic pollutants [18]. However, inorganic zeolites exhibit low adsorption of TcO_4^- even after modification [19] owing to electrostatic repulsion [20]. Organic anion exchange resins show higher TcO_4^- adsorption amounts, but they suffer from slow adsorption rates and long equilibrium times [21], which decreases the utilization efficiency of packed columns in fixed-bed treatment.

Both radiation stability and cost should be considered for commercial resins used for radionuclide removal. Therefore, radiation-resistant pyridyl-type resins, Reillex 425 series, have become the most popular resins for the adsorption of radioactive anions such as TcO_4^- [22, 23], compared to various recently developed functional groups [24–26]. As tertiary pyridyl groups must be protonated to gain electrostatic attraction with anions, quaternary pyridinium is more suitable for the removal of TcO_4^- (ReO_4^-) under neutral conditions [27, 28]. Furthermore, it is expected to provide more ion-exchange sites and thus increase the adsorption capacity by bonding another positive moiety onto the pyridinium via quaternization [29]. Commercial macroporous Reillex 425 resins, which are functionalized with pyridyl, have a large number of micropores inside the beads. In addition to the functional groups, the pore structure of resins is also essential for adsorption. Although abundant micropores provide a larger specific surface area and more adsorption sites, resulting in high adsorption amounts for adsorbents [30], they impede the diffusion of adsorbates, resulting in slower adsorption rates and longer equilibrium times [31]. Our previous work showed that appropriate dications could significantly promote the intraparticle diffusion of ReO_4^- anions in hierarchically mesoporous silica [32]. This indicates that it is possible to accelerate the transport of TcO_4^- inside micropores. Reillex 425 resins modified with suitable dications can potentially synchronously achieve high adsorption amounts and fast adsorption rates for TcO_4^-, which are important for the removal of TcO_4^- from treated water requiring secondary treatment.

In this study, we modified Reillex 425 resins with a series of dicationic pyridinium (DCP) derivatives integrating pyridinium and ammonium moieties ($Py^+C_nH_{2n}N^+Me_3$, where n represents the length of alkyl spacers between two positive N sites), which resulted in efficient adsorption of ReO_4^- and TcO_4^- by enhancing intraparticle diffusion. The adsorption isotherms and kinetics of different DCP-modified Reillex 425 were investigated to illustrate the adsorption mechanism and the effects of alkyl spacer lengths on adsorbate transfer. The effects of pH, salinity, and concentrations of interfering ions were studied to evaluate the potential of DCP-modified Reillex 425 for practical Tc removal.

2 Experimental section

2.1 Materials and chemicals

Detailed information on all materials and chemicals used in this work is provided in the Supporting Information. All materials and chemicals were used without further purification, except for the commercial Reillex 425 resins, which were washed to neutral pH (6–7) with ultrapure water.

2.2 Preparation of the modified Reillex 425

Reillex 425 resins (1.0 g) were dispersed in 50 mL of ethanol, followed by the addition of iodomethane (0.667 mL), (2-bromoethyl)trimethylammonium bromide (2-BETAB, 2.643 g), (3-bromopropyl)trimethylammonium bromide (3-BPTAB, 2.793 g), and (5-bromopentyl)trimethylammonium bromide (5-BPTAB, 3.093 g) to obtain the modified resins. These were labelled Reillex 425-Me, Reillex 425-C2, Reillex 425-C3, and Reillex 425-C5, respectively. The mixtures were heated to 60 °C in a water bath shaker (Changzhou Guoyu Instrument Manufacturing Co., Ltd, WHY-2) in the dark for six days. The products were purified by washing five times with ultrapure water and once with ethanol. Modified Reillex 425 resins were obtained by drying under vacuum (60 °C for 6 h).

2.3 Characterization of the adsorbents

Scanning electron microscopy (SEM, ZEISS, EVO 18, operating at 10 kV) was used to observe the morphologies of the resins. The specific surface areas and pore size distributions were calculated using the Brunauer–Emmett–

Teller and Barrett–Joyner–Halenda methods, respectively. This was done using the N_2 adsorption–desorption isotherms measured using a gas adsorption analyzer (Quantachrome Autosorb iQ, operating at 77 K). The chemical structures of the resins were characterized by solid-state ^{13}C cross-polarization magic angle spinning (CP-MAS) nuclear magnetic resonance (NMR) spectroscopy (Bruker AVANCE AV400 spectrometer), Fourier-transform infrared (FT-IR) spectroscopy (Thermo Nicolet 6700 spectrometer), and X-ray photoelectron spectroscopy (XPS, Thermo VG Scientific ESCALAB 250, equipped with a monochromatic Al K_α X-ray source at an energy of 1486.6 eV). A NanoBrook 90Plus PALS particle analyzer (Brookhaven Instruments) was used to measure the surface charges of the resins. Before measuring the zeta potential, the granular resins were ground into powders. 1.00 mg of each powder was soaked in 0.5 mL ethanol and subsequently diluted in 100 mL of water, yielding a concentration of 0.01 mg mL^{-1}.

2.4 Adsorption experiments

Batch adsorption experiments using ReO_4^- as an analog to radioactive TcO_4^- were conducted to evaluate the adsorption of different Reillex 425 resins. A single adsorption experiment was performed in 4 mL of Re solution (100 mg L^{-1}) containing 1.60 mg of adsorbent on a shaker. The solution pH was adjusted to the required value by adding negligible volumes (1 mol L^{-1}) of concentrated NaOH or HCl. The adsorbents were separated from the solution by filtration through a mixed cellulose ester membrane filter (0.22 μm) after adsorption. Equation 1 was used to calculate the equilibrium adsorption amount (q_e):

$$q_e = \frac{(c_0 - c_e) \times V}{m}, \quad (1)$$

where c_0 (mg L^{-1}) and c_e (mg L^{-1}) are the initial and equilibrium concentrations of adsorbate ions in the solution, respectively, both of which were obtained using an inductively coupled plasma optical emission spectrometer (ICP-OES, PerkinElmer Optima 7300DV), m (g) is the weight of the adsorbent, and V (L) is the volume of the solution.

In selective adsorption experiments, competitive anions, including I^- and $Sb(OH)_6^-$, were mixed with ReO_4^-. Re and Sb concentrations were measured using ICP-OES, and those of I^- were determined using an inductively coupled plasma mass spectrometer (ICP-MS, Thermo VG Scientific PlasmaQuad 3).

The reusability of the modified Reillex 425 was evaluated using adsorption–desorption cycles. The adsorbents were dispersed in 20 mL of HNO_3 (2 mol L^{-1}) and shaken for 6 h to desorb the ReO_4^-. The desorbed adsorbents were collected by precipitation and purified by washing with ultrapure water. The adsorption–desorption cycles were repeated five times.

Before the adsorption of TcO_4^-, 0.1 mL of NH_4TcO_4 stock solution was diluted by 1.9 mL of water, and mixed with 10 mL of Ultima Gold AB cocktail to determine the active concentration using a Packard Tri-Carb 2900 Liquid Scintillation Analyzer. The active ^{99}Tc concentration of the stock solution was 1250 Bq mL^{-1} (2 mg L^{-1}). The batch adsorption experiment for Tc was carried out in a TcO_4^- solution obtained by diluting the stock solution 10 times (125 Bq mL^{-1}) using the same procedure as for the adsorption of Re. After adsorption, 3 mL of the supernatant was mixed with 10 mL of Ultima Gold AB cocktail to measure the active concentration, and the Tc removal ratio was calculated using Eq. 2,

$$\text{Removal ratio} = \left(1 - \frac{A_t}{A_0}\right) \times 100\%, \quad (2)$$

where A_0 (Bq) and A_t (Bq) are the radioactivity of ^{99}Tc in solution before and after adsorption, respectively.

3 Results and discussion

3.1 Synthesis of the modified Reillex 425

Reillex 425 resins were modified via a simple quaternization reaction, as illustrated in Scheme 1. The operation strongly affected the morphologies of the obtained products. The resin granules became powders when the reaction was performed under stirring (Fig. S1), which is undesirable for column treatment of radioactive sewage. To avoid pulverization and maintain the granular appearance of the products, modification must be carried out using a shaker. As shown in Fig. 1a–e, although modification in a shaker roughened the resin surface, the modified Reillex 425 resins retained their spherical shape with an average bead size around 0.7 mm (Table 1). The resultant Reillex 425-C*n* (n = 2, 3, and 5, representing the number of carbon atoms between the pyridinium and ammonium moieties) showed the same color as the pristine Reillex 425 resin, whereas Reillex 425-Me turned yellow because of adsorption of iodine during modification [33]. All modified resins displayed the same type II N_2 adsorption–desorption isotherms as pristine Reillex 425 (Fig. 1f). In the high-relative-pressure region ($P/P_0 > 0.8$), the N_2 adsorption quantity increased sharply, confirming the macroporous structure [34]. The pore size distributions demonstrated that all the resins possessed hierarchically porous structures, integrating pores at different size scales, from macropores to micropores (Fig. 1g). The modification did

Scheme 1 Schematic illustration for the synthesis of Reillex 425-C*n* and Reillex 425-Me

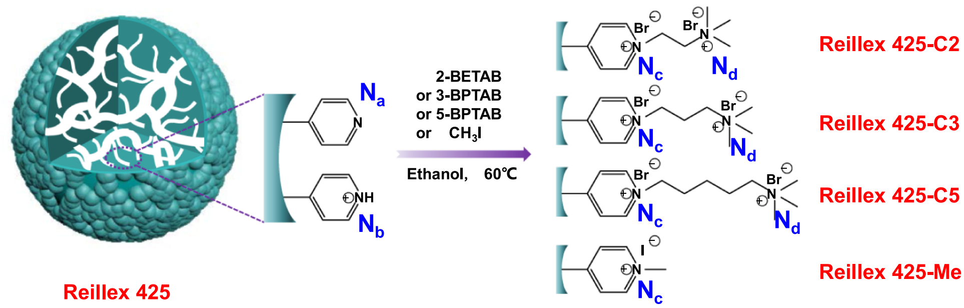

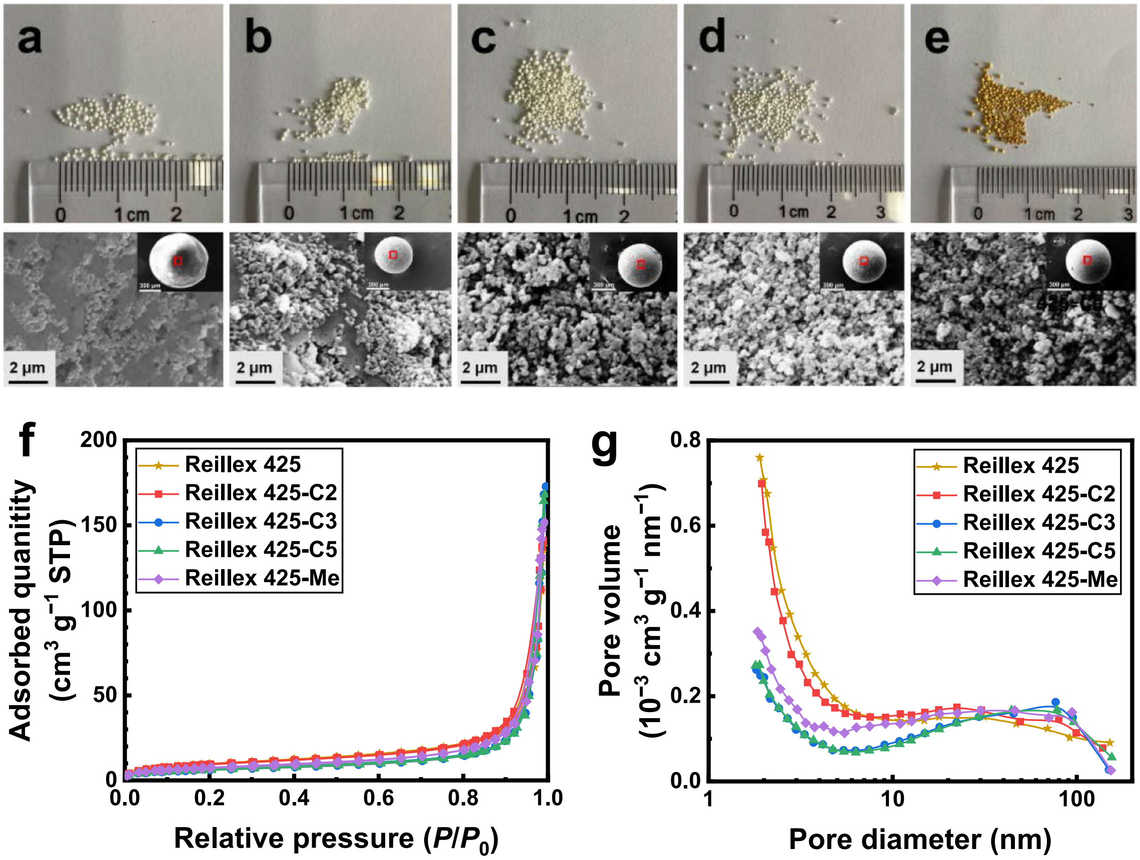

Fig. 1 Digital photographs and SEM images of Reillex 425 (**a**), Reillex 425-C2 (**b**), Reillex 425-C3 (**c**), Reillex 425-C5 (**d**), and Reillex 425-Me (**e**). All the scale bars in the insets of SEM images are 300 μm. N_2 adsorption–desorption isotherms (**f**) and the corresponding pore size distributions (**g**) of different resins

Table 1 Specific surface areas, pore volumes, modification efficiencies, and modification densities (ρ_m) of Reillex 425, Reillex 425-Cn, and Reillex 425-Me

	Reillex 425	Reillex 425-C2	Reillex 425-C3	Reillex 425-C5	Reillex 425-Me
Specific surface area (m^2 g^{-1})	35.48	34.92	24.14	23.89	28.06
Pore volume (cm^3 g^{-1})	0.21	0.22	0.27	0.26	0.24
Modification efficiency	–	13.0%	21.2%	26.6%	48.6%
ρ_m (mmol g^{-1})	7.143[a]	0.929[b]	1.517[b]	1.897[b]	3.474[b]

[a] This value refers to the moles of ($N_a + N_b$) per gram of Reillex 425 resin, which was estimated according to the content of 4-vinylpyridine in Reillex 425 resin (75 wt%)

[b] These values refer to the moles of N_c per gram of the Reillex 425-C*n* and Reillex 425-Me resins

not alter the specific surface areas and total pore volumes of the Reillex resins (Table 1), suggesting that the porous structure, which is beneficial for adsorption, was retained after modification. Moreover, the average pore width slightly increased after modification, which might have enhanced the mass transfer of the adsorbates.

The ^{13}C SSNMR spectra provided direct evidence for the successful modification of Reillex 425 resins. The characteristic peaks of poly(4-vinylpyridine) and polystyrene are shown in Fig. 2a. After tertiary pyridyl was quaternized with alkyltrimethylammonium, Reillex 425-C2 displayed three new peaks, ascribed to the carbon atoms in the spacer (C_{h1} and C_{h2}) and trimethylammonium moiety (C_i), at 45.2, 63.6, and 55.4 ppm, respectively. Similarly, the characteristic peaks of all other modified Reillex 425 could be identified in the corresponding ^{13}C SSNMR spectra. From the FT-IR spectra in Fig. 2b, the quaternization of pyridyl in Reillex 425 shifted the absorption peak for the in-plane C=C stretching vibration of the pyridyl ring from 1603 to 1637 cm^{-1} [35, 36]. Other peaks at 1419 (aromatic semicircle C=N stretching of the pyridyl ring), 2927, and 2972 cm^{-1} (stretching vibration of

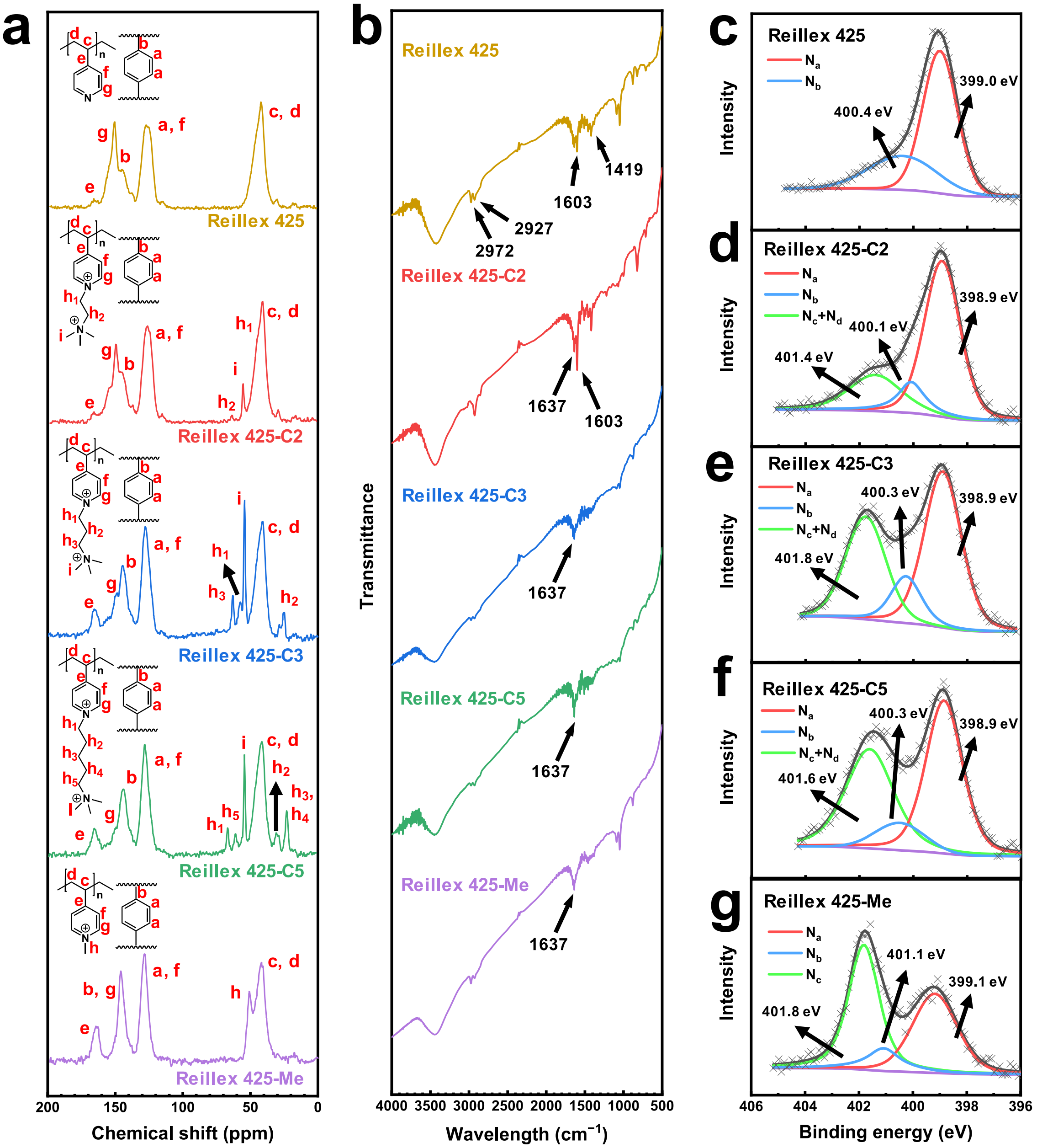

Fig. 2 ^{13}C CP-MAS SSNMR (**a**), FT-IR (**b**), and high-resolution XPS N 1 s spectra of Reillex 425 (**c**), Reillex 425-C2 (**d**), Reillex 425-C3 (**e**), Reillex 425-C5 (**f**), and Reillex 425-Me (**g**)

saturated C–H in the polymer main chain) remained the same [37]. Reillex 425-C2 simultaneously displayed two peaks at 1603 and 1637 cm^{-1}, and the other modified Reillex 425 only exhibited the latter peak, which implied that Reillex 425-C2 had a smaller quaternization efficiency than the other modified resins. XPS analysis of the valence states of the N atoms was performed to quantitatively estimate the modification efficiency. From the N 1 s spectrum (Fig. 2c), Reillex 425 only contains two types of nitrogen—N atoms at tertiary (399.0 eV) and protonated (400.4 eV) pyridyl. After quaternization, all the Reillex 425-C*n* displayed a new peak at higher binding energies around 401.5 eV, which was attributed to the quaternary N atoms in both pyridinium (N_c) and ammonium (N_d) moieties (Fig. 2d–f) [3]. The modification efficiency, defined as the ratio of N_c to ($N_a + N_b + N_c$) (*i.e.*, all N atoms in tertiary pyridyl, protonated pyridyl, and quaternary pyridinium), was estimated at 13.0, 21.2, and 26.6% for Reillex 425-C2, Reillex 425-C3, and Reillex 425-C5, respectively. Evidently, longer spacers reduce the electrostatic repulsion between the two positive N atoms in one DCP group, thus increasing the modification efficiency [38]. For comparison, Reillex 425-Me, in which the pyridyl groups were functionalized with methyl groups, was prepared. The smaller steric hindrance and weaker electrostatic repulsion of methyl-endowed Reillex 425-Me with a significantly higher modification efficiency of 48.6% (Fig. 2g). The modification densities (ρ_m, mmol g^{-1}, representing the moles of N_c per gram of resin) were estimated according to the modification efficiencies and the density of pyridyl in Reillex 425 (Table 1).

3.2 Adsorption of Re(VII) on the modified Reillex 425 resins

Re(VII) primarily exists as a perrhenate anion (ReO_4^-) over a pH range of 0 to 12 [39]; thus, its adsorption behavior is determined by the surface charge of the adsorbents. As shown in Fig. 3a, the zeta potential of the pristine Reillex 425 resin was positive at $pH < 3$ and negative at $pH > 5$ because of deprotonation of the pyridyl groups in the polymer ($pK_a = 5.6$) [40]. Consequently, the electrostatic repulsion between the resin and ReO_4^- gradually decreased when the pH decreased from 9 to 2. The q_e of Re on Reillex 425 reached a maximum of 194.8 mg g^{-1} at pH = 2 (Fig. 3b). However, if the pH is further decreased, the competitive adsorption of concentrated Cl^- anions would suppress ReO_4^- adsorption [41, 42]. After the tertiary pyridyl groups on Reillex 425 were quaternized, all the modified resins exhibited positive zeta potentials at pH 1–9 owing to the intrinsic positively charged N atoms. Although all Reillex 425-C*n* resins showed the same pH-dependent adsorption pattern as that of pristine Reillex 425 because of some remaining tertiary pyridyl, their q_e values were significantly enlarged under neutral conditions, remaining above 135.5 mg g^{-1}. Particularly, Reillex 425-C3 and Reillex 425-C5 exhibited larger q_e values than Reillex 425-C2 because of their higher modification efficiencies (Table 1). Reillex 425-Me showed almost the same adsorption amount as Reillex 425-C5 owing to its higher modification efficiency, even though the methyl pyridinium group had only one binding site. Notably, the morphology of the modified Reillex 425 greatly impacted the adsorption performance. The modified Reillex 425 powders obtained under stirring exhibited a dramatically decreased q_e under neutral conditions compared to the Reillex 425-C*n* beads (Fig. S2). Maintaining the granular shape during the modification not only increases the adsorption amount but also benefits column treatment for sewage.

To elucidate the adsorption mechanism for ReO_4^- on the modified Reillex 425 resins, the adsorption isotherms were investigated and analyzed using the Langmuir and Freundlich models (Fig. 4). The linear forms are given by Eqs. S(1) and (2), respectively, in the Supporting Information. From Table 2, the Langmuir model describes the adsorption of ReO_4^- on all the modified Reillex 425 resins, which suggests monolayer adsorption. The maximum adsorption capacities (q_m) were calculated to be 344.8, 416.7, 588.2, and 625.0 mg g^{-1} (1.852, 2.240, 3.159, and 3.360 mmol g^{-1}) for Reillex 425-C2, Reillex 425-C3, Reillex 425-C5, and Reillex 425-Me, respectively. Compared with other adsorbents listed in Table S1, the higher q_m of modified Reillex 425 favors an extended lifetime of the packed column. It is evident that q_m on Reillex 425-Me equaled its ρ_m, suggesting that all positively charged N atoms were occupied by ReO_4^-. Meanwhile, all q_e values for Reillex 425-C*n* were higher than their ρ_m values, ranging from 1.5 to 2 times, indicating that ammonium and pyridinium sites should be capable of adsorbing ReO_4^- simultaneously. The q_m of Reillex 425-C2 was twice its ρ_m, demonstrating that all adsorption sites on the DCP groups could be utilized. However, it seemed that not all the positively charged sites on Reillex 425-C3 and Reillex 425-C5 were accessible at q_m/ρ_m ratios below 2, indicating that the adsorption of ReO_4^- anions inside the micropores might be hindered.

The adsorption thermodynamics were further investigated to gain a better understanding of the different adsorption patterns between the different DCP groups. Reillex 425-C2 and 425-C5, which contained the shortest and longest spacers, respectively, were selected as representatives. The changes in the standard Gibbs free energy (ΔG^0), enthalpy (ΔH^0), and entropy (ΔS^0) of adsorption were calculated using Eq. S(3) and S(4) (Supporting Information), respectively. From Fig. 5 and the calculated

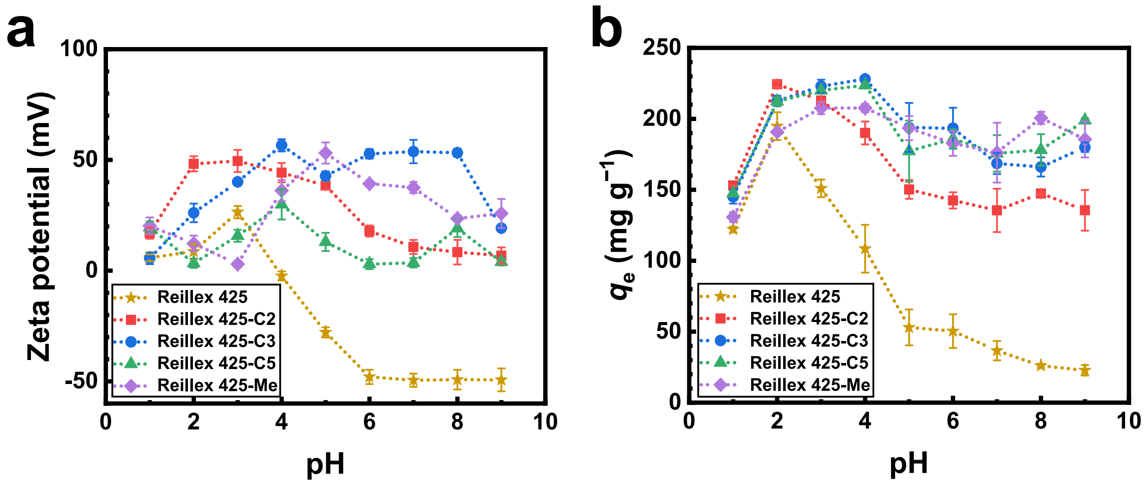

Fig. 3 Zeta potentials (**a**) and Re adsorption amounts (**b**) of different Reillex 425 resins at different initial pH (adsorbent dosage = 0.4 g L^{-1}, $[\text{Re}]_0$ = 100 mg L^{-1}, T = 298 ± 1 K, t = 12 h)

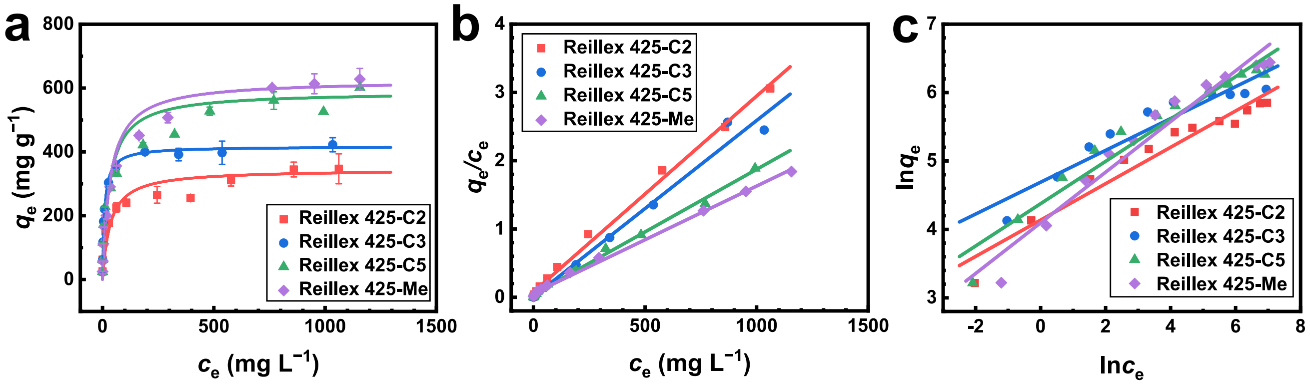

Fig. 4 The adsorption isotherms of ReO_4^- on Reillex 425-C*n* and Reillex 425-Me (**a**) fitted by Langmuir (**b**) and Freundlich models (**c**). The solid curves in (**a**) are the fitting curves by the Langmuir model (adsorbent dosage = 0.4 g L^{-1}, $[\text{Re}]_0$ = 10–1400 mg L^{-1}, initial pH = 6.6–6.8, T = 298 ± 1 K, t = 12 h)

Table 2 Isotherm parameters for the adsorption of ReO_4^- on Reillex 425-C*n* and Reillex 425-Me calculated by Langmuir and Freundlich models

	Langmuir			Freundlich		
	q_m (mg g^{-1})	k_L[a] (L mg^{-1})	R^2	n[b]	k_F[c] (mg g^{-1})(L mg^{-1})$^{1/n}$	R^2
Reillex 425-C2	344.8	0.0368	0.9952	3.691	62.49	0.9512
Reillex 425-C3	416.7	0.1127	0.9990	4.290	108.96	0.9534
Reillex 425-C5	588.2	0.0322	0.9913	3.232	79.52	0.9466
Reillex 425-Me	625.0	0.0289	0.9975	2.701	60.09	0.9508

[a] k_L is the equilibrium constant for the Langmuir model

[b] n is a constant reflecting the favorability of the adsorption process in the Freundlich model

[c] k_F is the equilibrium constant for the Freundlich model

results in Table 3, the negative ΔH^0 and ΔG^0 values demonstrated that the spontaneous adsorption of ReO_4^- on both Reillex 425-C2 and 425-C5 was exothermic. A lower temperature benefits the adsorption process, as q_e and ΔG display negative and positive correlations with temperature, respectively. Adsorption of ReO_4^- on Reillex 425-C5 was more thermodynamically favorable as its ΔG^0 was more negative than that of Reillex 425-C2. However, the adsorption isotherms showed that Reillex 425-C5 had a lower utilization rate for binding sites. Thus, ReO_4^- adsorption on Reillex 425-C5 is controlled by kinetics rather than thermodynamics. Meanwhile, kinetics had less effect on ReO_4^- adsorption for Reillex 425-C2.

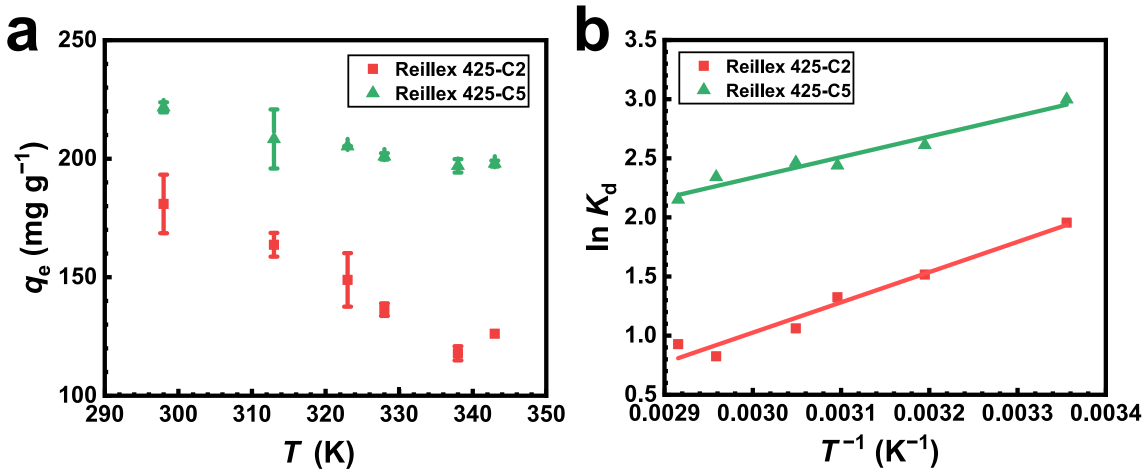

Fig. 5 Adsorption amounts of Re on Reillex 425-C2 and Reillex 425-C5 at different temperatures (**a**). The fitting plots of ln K_d versus T^{-1} (**b**) (adsorbent dosage = 0.4 g L^{-1} [Re]$_0$ = 100 mg L^{-1}, initial pH = 6.6–6.8, t = 12 h)

Table 3 Thermodynamic parameters for the adsorption of ReO_4^- on Reillex 425-C2 and Reillex 425-C5

	ΔH^0	ΔS^0	ΔG^0 (kJ mol^{-1})						R^2
	(kJ mol^{-1})	(J mol^{-1})	298 K	313 K	323 K	328 K	338 K	343 K	
Reillex 425-C2	− 21.28	− 55.30	− 4.796	− 3.967	− 3.414	− 3.137	− 2.585	− 2.308	0.9614
Reillex 425-C5	− 14.43	− 23.86	− 7.318	− 6.960	− 6.721	− 6.602	− 6.363	− 6.244	0.9535

A kinetic study demonstrated that Reillex 425-C2 showed a faster adsorption rate than Reillex 425-Me and all other Reillex 425-C*n*, reducing the equilibrium time for adsorption from 5 to 1 h (Fig. 6a). This agrees with the deduction that the adsorption of ReO_4^- on Reillex 425-C2 was less controlled by kinetics than on other Reillex 425-C*n*. Pseudo-first-order and pseudo-second-order kinetic models were used to quantitatively investigate the adsorption kinetics, the linear forms of which are given by Eqs. S(5) and (6) in Supporting Information, respectively. Figure 6b and c show the linear fitting curves of these two models, whose fitting results are listed in Table 4. The adsorption behavior of ReO_4^- can be described better by the pseudo-second-order kinetic model with a higher R^2, revealing that the adsorption is chemisorption [43]. Reillex 425-C2 exhibited a high adsorption rate constant k_2 of 0.00260 g mg^{-1} min^{-1}, which was more than six times larger than that of the other modified Reillex 425.

The adsorption process consists of four sequential stages: bulk diffusion, boundary layer diffusion, intraparticle diffusion, and surface reactions [44]. In batch adsorption experiments, the resistance to bulk diffusion is negligible because of the small concentration gradient of the adsorbate caused by vigorous shaking. The final stage of the adsorption reaction is nearly immediate for ion exchange and can be neglected. Therefore, the rate of the entire adsorption process is typically limited by the boundary layer and/or intraparticle diffusion stages. Equation (3) depicts the intraparticle diffusion model proposed by Weber and Morris [45].

$$q_t = k_p t^{1/2} + c_p, \tag{3}$$

where the slope k_p (mg g^{-1} min$^{-1/2}$) and intercept c_p (mg g^{-1}) are the rate constants of intraparticle diffusion and a constant related to the thickness of the boundary layer, respectively.

Piecewise linear regression suggested that the q_t *vs.* $t^{1/2}$ plots of both Reillex 425-C2 and Reillex 425-C5 showed a two-stage adsorption pattern. The first stage agrees with the intraparticle diffusion model, with an intercept of almost 0, indicating that the adsorption of ReO_4^- on modified Reillex 425 is only controlled by intraparticle diffusion (Fig. 6d) [46]. The second stage displayed almost constant adsorption amounts, demonstrating that adsorption approached equilibrium. Thus, the higher adsorption rate of ReO_4^- on Reillex 425-C2 is attributed to the faster diffusion of ReO_4^- anions inside the micropores.

As demonstrated above, all Reillex 425-C*n* samples retained an almost unchanged pore structure. The difference between the $–Py^+C_2H_4N^+Me_3$ and

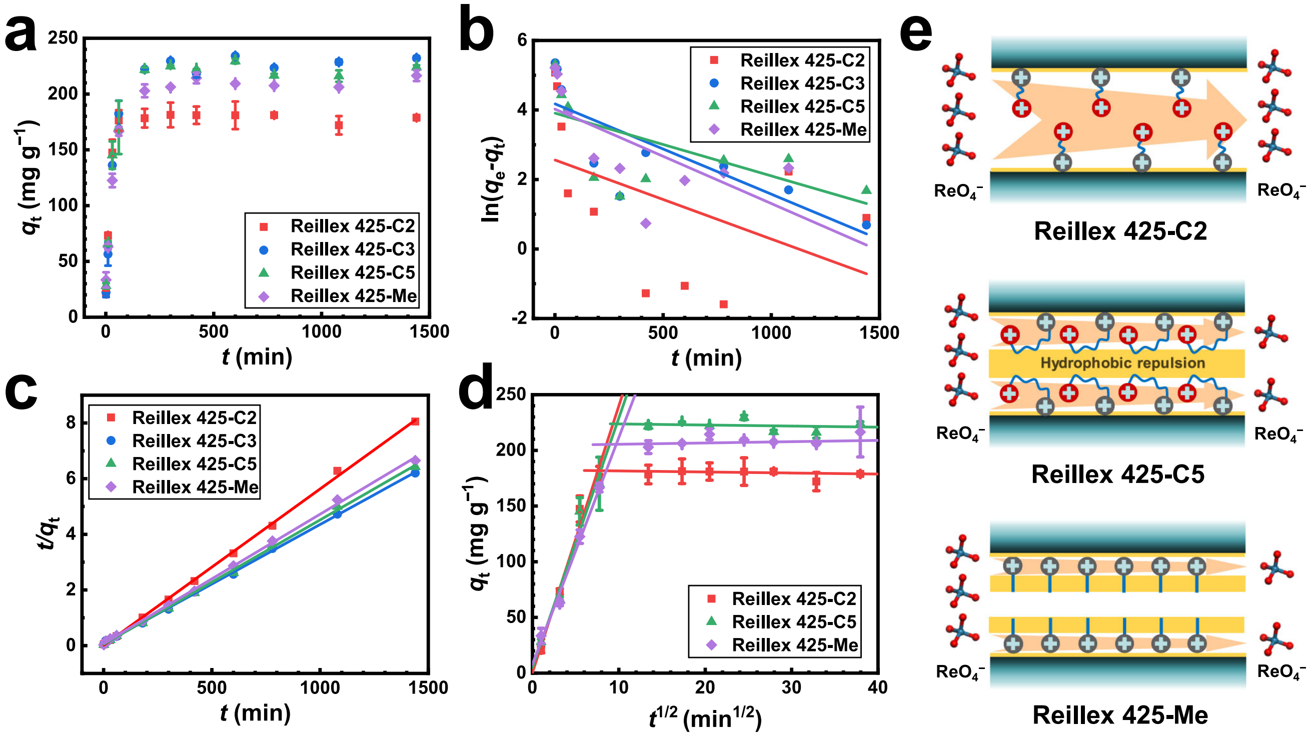

Fig. 6 The dynamic adsorption amounts of ReO_4^- by different modified Reillex 425 resins (**a**). Linear fitting by pseudo-first-order (**b**) and pseudo-second-order kinetic models (**c**). Analysis of the kinetics for ReO_4^- adsorption on Reillex 425-C2 and Reillex 425-C5 by intraparticle diffusion model (**d**) (adsorbent dosage = 0.4 g L^{-1}, $[Re]_0$ = 100 mg L^{-1}, initial pH = 6.6–6.8, T = 298 ± 1 K). The proposed transport pathways of ReO_4^- inside the micropores of Reillex 425-C2, Reillex 425-C5, and Reillex 425-Me (**e**)

Table 4 Kinetic parameters for the adsorption of ReO_4^- on different Reillex 425 resins

	Pseudo-first-order			Pseudo-second-order		
	$q_{e,\ cal}$[a] (mg g^{-1})	k_1[b] (min^{-1})	R^2	$q_{e,\ cal}$[a] (mg g^{-1})	k_2[c] (g mg^{-1} min^{-1})	R^2
Reillex 425-C2	12.95	0.00227	0.1334	177.94	0.00260	0.9990
Reillex 425-C3	65.16	0.00260	0.6152	233.64	0.00024	0.9993
Reillex 425-C5	49.91	0.00181	0.3215	223.71	0.00043	0.9989
Reillex 425-Me	56.01	0.00272	0.3886	215.05	0.00028	0.9990

[a] $q_{e,\ cal}$ is the adsorption amount at equilibrium calculated using the corresponding adsorption kinetic model

[b] k_1 is the adsorption rate constant of the pseudo-first-order kinetic model

[c] k_2 is the adsorption rate constant of the pseudo-second-order kinetic model

$–Py^+C_5H_{10}N^+Me_3$ groups or, more accurately, the different spacers are presumed to drastically affect anion transport inside the microporous channels of Reillex 425-C*n*. The longer alkyl spacers were more flexible, which enabled greater changes in the conformation of the DCP groups. It is possible to rearrange the pyridinium and ammonium sites vertically owing to the electrostatic repulsion between them and the hydrophobic aggregation of the long carbon spacers, as illustrated in Fig. 6e. Under such circumstances, the adsorption of ReO_4^- at the first cationic site impedes the diffusion of ReO_4^- towards the second cationic moiety [47]. Furthermore, the aggregation of long and flexible carbon chains forms hydrophobic microphases inside microporous channels, which increases the resistance of intraparticle diffusion of hydrophilic species such as hydrated anions [48]. Therefore, steric hindrance and hydrophobic repulsion generated by the longer spacer of the $–Py^+C_5H_{10}N^+Me_3$ groups retard ReO_4^- transport inside the micropores of Reillex 425-C5. For Reillex 425-C2, the two positive charges connected by shorter alkyl spacers tended to be laterally arranged (Fig. 6e), leading to smaller steric hindrance. Moreover, hydrophobic microphases are not formed due to repulsion among the positive charges. As a result, the transport of ReO_4^- anions inside the microporous channels modified with $Py^+C_2H_4N^+Me_3$ groups was enhanced. Reillex 425-Me functionalized with monocationic methyl pyridinium also exhibited a slower adsorption rate than Reillex 425-C2, although no spacers were present. This is because the quaternization of pyridyl with methyl increases the hydrophobicity of the surface of the microporous channels, hindering the intraparticle diffusion of ReO_4^- (Fig. 6e) [49]. According to the above discussion, dicationic –$Py^{+-}C_2H_4N^+Me_3$ groups with short spacers can promote the transportation of ReO_4^- inside the microporous channels.

To evaluate the contribution of DCP groups to practical Tc removal, the adsorption kinetics of TcO_4^- on different modified Reillex 425 samples were further investigated. As displayed in Fig. 7a, all the modified Reillex 425 resins remove approximately 99% of the Tc due to its trace concentration of 125 Bq mL^{-1} (0.2 mg L^{-1} of ^{99}Tc). Reillex 425-C2 still exhibited the fastest adsorption rate, with the highest 1-h removal ratio of 93.5%. Tc removal accelerated by the –$Py^+C_2H_4N^+Me_3$ groups was verified by kinetic analysis. The adsorption kinetics followed a pseudo-second-order kinetic model (Fig. 7b and c), similar to that of ReO_4^-. Reillex 425-C2 showed the largest k_2 of 0.211 g mg^{-1} min^{-1} among all three Reillex 425-Cn samples (Table 5).

TcO_4^- adsorption on Reillex 425-Me was faster than that on Reillex 425-C2, which was different from the adsorption of ReO_4^-. Piecewise linear regression of the kinetic data using the intraparticle diffusion model validated that the adsorption of TcO_4^- on Reillex 425-Cn showed the same pattern as that of ReO_4^-, only controlled by intraparticle diffusion (Table 6). However, TcO_4^- adsorption on Reillex 425-Me is controlled by both stages of the boundary layer and intraparticle diffusion. After obtaining the intercept c_p in the intraparticle diffusion model by linear fitting of the first stage, an initial adsorption factor (R_i), defined by the following Eq. 4 can be calculated to distinguish the contributions from different diffusion processes. R_i was 0.772 for Reillex 425-Me, implying that 77.2% of the TcO_4^- adsorption was governed by intraparticle diffusion. The remaining 22.8% occurs almost instantaneously, as determined by boundary

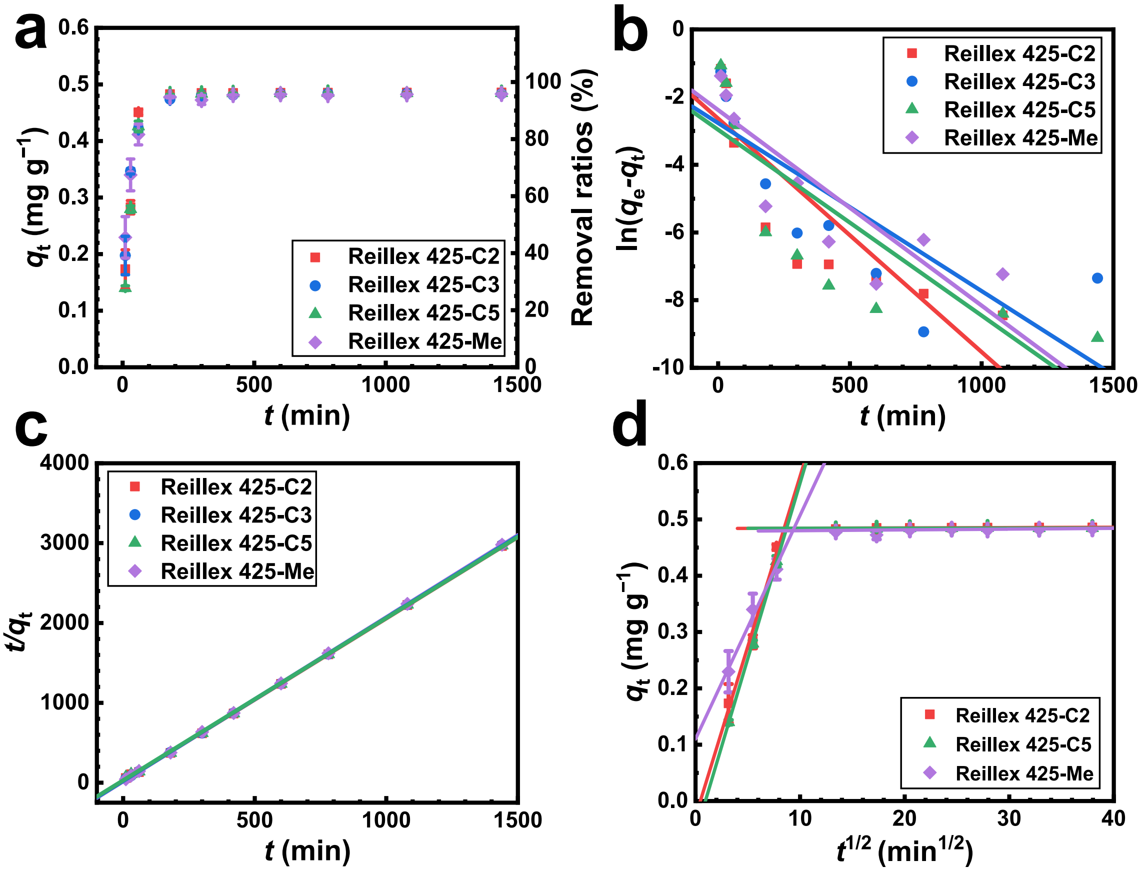

Fig. 7 The dynamic adsorption amounts and removal ratios of TcO_4^- on different modified Reillex 425 resins (**a**). Linear fitting by pseudo-first-order (**b**) and pseudo-second-order kinetic models (**c**). Analysis of the kinetics for TcO_4^- adsorption on Reillex 425-C2 and Reillex 425-C5 by intraparticle diffusion model (**d**) (adsorbent dosage = 0.4 g L^{-1}, $[Tc]_0$ = 0.2 mg L^{-1}, initial pH = 6.6–6.8, T = 298 ± 1 K)

Table 5 Kinetic parameters for the adsorption of TcO_4^- on different Reillex 425 resins

	Pseudo-first-order			Pseudo-second-order		
	$q_{e,\ cal}$ (mg g^{-1})	k_1 (min^{-1})	R^2	$q_{e,\ cal}$ (mg g^{-1})	k_2 (g mg^{-1} min^{-1})	R^2
Reillex 425-C2	7.18	0.00690	0.7340	0.45	0.21118	0.9998
Reillex 425-C3	6.28	0.00496	0.6393	0.49	0.19431	0.9999
Reillex 425-C5	5.17	0.00549	0.6725	0.49	0.13911	0.9997
Reillex 425-Me	9.24	0.00578	0.7399	0.49	0.24657	0.9999

Table 6 Kinetic parameters for the adsorption of ReO_4^- and TcO_4^- on different modified Reillex 425 resins fitted by Weber–Morris intraparticle diffusion model

	ReO_4^-				TcO_4^-			
	k_p (mg g^{-1} $min^{-1/2}$)	c_p	R^2	R_i	k_p (mg g^{-1} $min^{-1/2}$)	c_p	R^2	R_i
Reillex 425-C2	24	0.3963	0.9756	0.9978	0.061	− 0.0279[a]	0.9839	≈ 1[b]
Reillex 425-C5	22	4.9986	0.9643	0.9782	0.062	− 0.0589[a]	0.9996	≈ 1[b]
Reillex 425-Me	20	7.8633	0.9885	0.9633	0.040	0.1101	0.9863	0.7721

[a,b] The fitting intercept c_p became negative owing to experimental errors and thus R_i could be regarded as its maximum value of 1

layer diffusion [50]. Reillex 425-C2 exhibited a 52.5% higher k_p than Reillex 425-Me, demonstrating that the –$Py^+C_2H_4N^+Me_3$ groups also accelerated the adsorption of TcO_4^- by promoting intraparticle diffusion. Generally, higher mass transfer rates shorten the mass transfer zone when adsorbents are packed in a column. In other words, the difference between breakthrough and equilibrium times is reduced, resulting in a steeper breakthrough curve. Consequently, fixed-bed columns can be utilized more efficiently.

$$R_i = 1 - \frac{c_p}{q_e} \tag{4}$$

Although the contaminated seawater in Fukushima Daiichi nuclear power station has been desalinated during the treatment, the treated water still contains Cl^- (1900 mg L^{-1}, or 5.4×10^{-2} mol L^{-1}) and SO_4^{2-} (610 mg L^{-1}, or 6.4×10^{-3} mol L^{-1}) [51], the two main anions in seawater [52], which may hamper the adsorption of TcO_4^-. In 0.05 mol L^{-1} of Cl^- or SO_4^{2-}, the q_e of Re on Reillex 425-C2 decreased to 64.9 and 49.7% of the original value, respectively, owing to competitive adsorption by the DCP groups (Fig. 8a). With an increase in the anion concentration, Cl^- and SO_4^{2-} had different effects on Re adsorption. q_e declined to 25.8% in 1 mol L^{-1} of Cl^-, while it remained almost the same (44.8%) in 1 mol L^{-1} of SO_4^{2-}. Reillex 425-C5 showed a similar trend; q_e decreased from 72.1 to 28.3% in Cl^- but remained constant at approximately 65.0% in SO_4^{2-} as the anion concentration rose from 0.05 to 1 mol L^{-1}(Fig. 8b). Because of the hydrophobic nature of the Reillex 425 resin matrix, the inner walls of the porous channels should retain a certain hydrophobicity even after the dication modification. The hydration energies for the different anions follow the order SO_4^{2-} (− 1080 kJ mol^{-1}) < Cl^- (− 340 kJ mol^{-1})-< ReO_4^- (− 330 kJ mol^{-1}) [53]. Therefore, SO_4^{2-}, which is more hydrophilic, has less influence on ReO_4^- adsorption. Reillex 425-C5, containing hydrophobic microphases formed by longer and more flexible carbon chains, is more resistant to these hydrophilic anions than Reillex 425-C2 for the same reason. In addition to Cl^- or SO_4^{2-}, the treated water also contains trace amounts of other radioactive anions, such as $^{129}I^-$ and $^{125}Sb(OH)_6^-$ [54]. Reillex 425-C2 and Reillex 425-C5 showed separation factors (S) between Re and I ($S_{Re/I} = K_{d,Re}/K_{d,I}$) of over 4.6 and 5.0, and $S_{Re/Sb}$ ($S_{Re/Sb} = K_{d,Re}/K_{d,Sb}$) of over 14.7 and 64.2, respectively, demonstrating their ability to remove TcO_4^- selectively from the treated water in Fukushima (Fig. 8c). After the adsorption of ReO_4^-, the used Reillex 425-Cn could be easily regenerated by HNO_3, with q_e remaining over 95% after five adsorption–desorption cycles (Fig. 8d).

4 Conclusion

In this study, we propose a simple and efficient method for improving the adsorption performance of ReO_4^- and TcO_4^- on Reillex 425 anion exchange resins by modifying them with a series of DCP groups. After modification, the obtained Reillex 425-Cn gained higher adsorption amounts for Re ($q_e > 135.0$ mg g^{-1}) in neutral solutions owing to the positively charged quaternary N sites in the DCP groups. The DCP integrated one quaternary pyridinium and

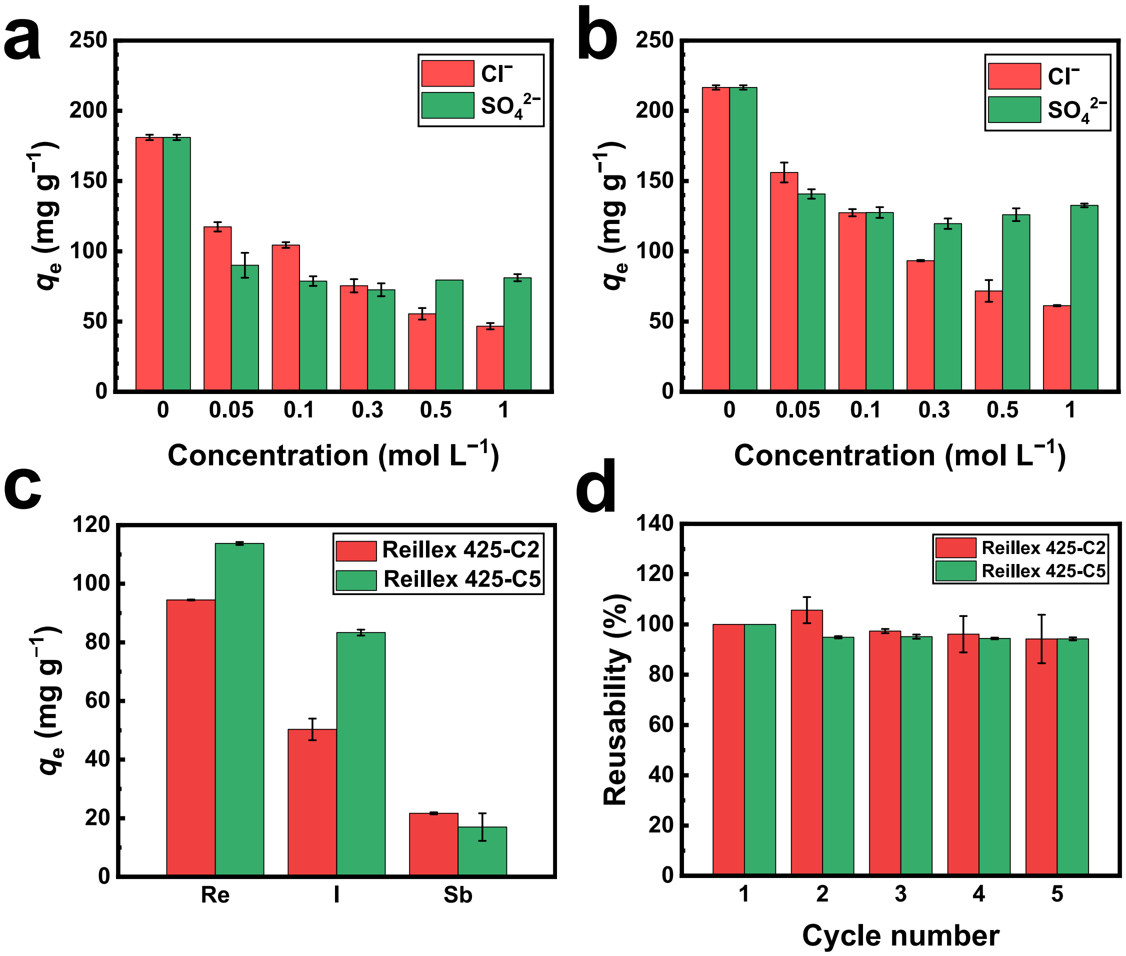

Fig. 8 Adsorption amounts of Re on Reillex 425-C2 (**a**) and Reillex 425-C5 (**b**) at different concentrations of Cl$^-$ and SO$_4^{2-}$ (adsorbent dosage = 0.4 g L^{-1}, [Re]$_0$ = 100 mg L^{-1}, T = 298 ± 1 K, initial pH = 6.6–6.8, t = 12 h). The adsorption selectivity of ReO$_4^-$ toward I$^-$ and Sb(OH)$_6^-$ on Reillex 425-C2 and Reillex 425-C5 (**c**) (adsorbent dosage = 0.4 g L^{-1}, [Re]$_0$ = [I]$_0$ = [Sb]$_0$ = 50 mg L^{-1}, T = 298 ± 1 K, initial pH = 6.6–6.8, t = 12 h). Reusability of Reillex 425-C2 and Reillex 425-C5 (**d**) (adsorbent dosage = 0.4 g L^{-1}, [Re]$_0$ = 100 mg L^{-1}, T = 298 ± 1 K, initial pH = 6.6–6.8, t = 6 h)

one quaternary ammonium into a single group, both of which adsorbed ReO$_4^-$ simultaneously. Consequently, the maximum Re adsorption capacities, q_m, for Reillex 425-C2, Reillex 425-C3, and Reillex 425-C5 reached as high as 344.8, 416.7, and 588.2 mg g^{-1}, respectively. A detailed study of the adsorption isotherms revealed that the utilization ratio of all the adsorption sites only ranged from 75 to 100% at saturated adsorption, depending on the length of the alkyl spacers between the two positive charges in the DCP group. A longer spacer was found to be more thermodynamically favorable for Re adsorption. Thus, it can be concluded that adsorption is kinetically controlled. Reillex 425-C2 exhibited an adsorption rate six times faster than those of Reillex 425-Cn and Reillex-425-Me. A deeper investigation into the mass transfer mechanism of the adsorbates illustrated that the adsorption of ReO$_4^-$ on modified Reillex 425 was only governed by intraparticle diffusion. The enhanced transport of ReO$_4^-$ anions inside the microporous channels of the resins is responsible for the accelerated adsorption on Reillex 425-C2. For Reillex 425-C5, longer alkyl spacers might result in the perpendicular distribution of the two positive charges and the formation of hydrophobic microphases by carbon chain aggregation. This sterically hinders the anion from approaching the second cation and repels the hydrated ReO$_4^-$ anions. Contrarily, the two positive charges in the –Py$^+$C$_2$H$_4$N$^+$Me$_3$ groups with shorter alkyl spacers may be arranged laterally, generating no hydrophobic microphases. The smaller steric hindrance and repulsion promoted the intraparticle diffusion of ReO$_4^-$ inside the Reillex 425-C2 resins. For the adsorption of radioactive TcO$_4^-$ at trace concentrations, Reillex 425-C2 showed the same adsorption pattern dictated only by intraparticle diffusion. The –Py$^+$C$_2$H$_4$N$^+$Me$_3$ groups enhanced the mass transfer of TcO$_4^-$ inside the resin beads. In addition to rapid adsorption, Reillex 425-C2 also exhibited several other features that benefit the removal or remediation of TcO_4^- from treated water, which contains various non-tritium radioisotopes beyond the regulatory standard for discharge. These include exothermic adsorption, good selectivity, excellent reusability, and adequate salinity tolerance. The modification strategy with appropriate dications should increase the utilization efficiency of the fixed-bed column by accelerating the transport of TcO_4^- anions inside the micropores of the filling resins, which implies enormous environmental and economic benefits.

Authors contribution All authors contributed to the study conception and design. Material preparation, data collection, and analysis were performed by Peng Zhang, Yi-Zhi Chen, Han-Qin Weng, Zi-Fang Guo, Jia-Liang Chen, Xing Zhao, Guo-An Ye, and Ming-Zhang Lin. The first draft of the manuscript was written by Peng Zhang and Han-Qin Weng, and all authors commented on previous versions of the manuscript. All authors read and approved the final manuscript.

References

1. D. Parajuli, H. Tanaka, Y. Hakuta et al., Dealing with the aftermath of Fukushima Daiichi nuclear accident: decontamination of radioactive cesium enriched ash. Environ. Sci. Technol. **47**, 3800–3806 (2013). https://doi.org/10.1021/es303467n
2. G. Steinhauser, Fukushima's forgotten radionuclides: a review of the understudied radioactive emissions. Environ. Sci. Technol. **48**, 4649–4663 (2014). https://doi.org/10.1021/es405654c
3. P. Xiao, D. Han, M. Zhai et al., Comparison with adsorption of Re(VII) by two different γ-radiation synthesized silica-grafting of vinylimidazole/4-vinylpyridine adsorbents. J. Hazard. Mater. **324**, 711–723 (2017). https://doi.org/10.1016/j.jhazmat.2016.11.045
4. I.T. Burke, C. Boothman, J.R. Lloyd et al., Effects of progressive anoxia on the solubility of technetium in sediments. Environ. Sci. Technol. **39**, 4109–4116 (2005). https://doi.org/10.1021/es048124p
5. G. Lear, J.M. McBeth, C. Boothman et al., Probing the biogeochemical behavior of technetium using a novel nuclear imaging approach. Environ. Sci. Technol. **44**, 156–162 (2010). https://doi.org/10.1021/es802885r
6. T.M. Gilliam, R.D. Spence, W.D. Bostick et al., Solidification/stabilization of technetium in cement-based grouts. J. Hazard. Mater. **24**, 189–197 (1990). https://doi.org/10.1016/0304-3894(90)87009-7
7. Update of Decommissioning and Reconstruction—Fukushima Daiichi NPS in 2021. Ministry of Economy, Trade and Industry, https://www.meti.go.jp/english/earthquake/nuclear/decommissioning/pdf/02_meti_sideevent.pdf. Accessed 6 September 2021
8. K.O. Buesseler, Opening the floodgates at Fukushima. Science **369**, 621 (2020). https://doi.org/10.1126/science.abc1507
9. J.S. McCloy, B.J. Riley, A. Goel et al., Rhenium solubility in borosilicate nuclear waste glass: implications for the processing and immobilization of technetium-99. Environ. Sci. Technol. **46**, 12616–12622 (2012). https://doi.org/10.1021/es302734y
10. T. Suzuki, Y. Fujii, W. Yan et al., Adsorption behavior of VII group elements on tertiary pyridine resin in hydrochloric acid solution. J. Radioanal. Nucl. Chem. **282**, 641 (2009). https://doi.org/10.1007/s10967-009-0165-9
11. J. Zu, R. Liu, J. Zhang et al., Adsorption of Re and ^{99}Tc by means of radiation-grafted weak basic anion exchange resi. J. Radioanal. Nucl. Chem. **310**, 229–237 (2016). https://doi.org/10.1007/s10967-016-4819-0
12. P.Y. Wang, J.H. Zu, Y.Z. Wei, Synthesis and characterization of porous 4VP-based adsorbent for Re adsorption as analogue to ^{99}Tc. Nucl. Sci. Tech. **28**, 30 (2017). https://doi.org/10.1007/s41365-017-0181-3
13. L. Zhu, D. Sheng, C. Xu et al., Identifying the recognition site for selective trapping of $^{99}TcO_4^-$ in a hydrolytically stable and radiation resistant cationic metal–organic framework. J. Am. Chem. Soc. **139**, 14873–14876 (2017). https://doi.org/10.1021/jacs.7b08632
14. A. Thevenet, C. Marie, C. Tamain et al., Perrhenate and pertechnetate complexation by an azacryptand in nitric acid medium. Dalton Trans. **49**, 1446–1455 (2020). https://doi.org/10.1039/C9DT04314D
15. Y. Wang, Z. Wu, H. Weng et al., Separation of Re(VII) from aqueous solution by acetone-enhanced photoreduction: an insight into the role of acetone. J. Photochem. Photobiol. A Chem. **380**, 111823 (2019). https://doi.org/10.1016/j.jphotochem.2019.04.034
16. Y. Shang, J. Xiao, H. Weng et al., Efficient separation of Re(VII) by radiation-induced reduction from aqueous solution. Chem. Eng. J. **341**, 317–326 (2018). https://doi.org/10.1016/j.cej.2018.02.022
17. M.K. Uddin, A review on the adsorption of heavy metals by clay minerals, with special focus on the past decade. Chem. Eng. J. **308**, 438–462 (2017). https://doi.org/10.1016/j.cej.2016.09.029
18. J. Lehto, R. Koivula, H. Leinonen et al., Removal of radionuclides from Fukushima Daiichi waste effluents. Sep. Purif. Rev. **48**, 122–142 (2019). https://doi.org/10.1080/15422119.2018.1549567
19. D. Li, D.I. Kaplan, A.S. Knox et al., Aqueous ^{99}Tc, ^{129}I and ^{137}Cs removal from contaminated groundwater and sediments using highly effective low-cost sorbents. J. Environ. Radioact. **136**, 56–63 (2014). https://doi.org/10.1016/j.jenvrad.2014.05.010
20. C.D. Williams, P. Carbone, Selective removal of technetium from water using graphene oxide membranes. Environ. Sci. Technol. **50**, 3875–3881 (2016). https://doi.org/10.1021/acs.est.5b06032
21. L. Liang, B. Gu, X. Yin, Removal of technetium-99 from contaminated groundwater with sorbents and reductive materials. Sep. Technol. **6**, 111–122 (1996). https://doi.org/10.1016/0956-9618(96)00148-8
22. K. Pillay, A review of the radiation stability of ion exchange materials. J. Radioanal. Nucl. Chem. **102**, 247–268 (1986). https://doi.org/10.1007/BF02037966
23. M. Nogami, Y. Fujii, T. Sugo, Radiation resistance of pyridine type anion exchange resins for spent fuel treatment. J. Radioanal. Nucl. Chem. **203**, 109–117 (1996). https://doi.org/10.1007/BF02060385
24. Y. Wang, D. Han, S. Zhong et al., Quaternary phosphonium modified cellulose microsphere adsorbent for ^{99}Tc decontamination with ultra-high selectivity. J. Hazard. Mater. **401**, 123354 (2021). https://doi.org/10.1016/j.jhazmat.2020.123354
25. M. Ding, L. Chen, Y. Xu et al., Efficient capture of Tc/Re(VII, IV) by a viologen-based organic polymer containing tetraaza macrocycles. Chem. Eng. J. **380**, 122581 (2020). https://doi.org/10.1016/j.cej.2019.122581
26. Z. Dong, W. Yuan, Y. Li et al., Radiation synthesis of crown ether functionalized microcrystalline cellulose as bifunctional adsorbent: a preliminary investigation on its application for removal of ReO_4^- as analogue for TcO_4^-. Radiat. Phys. Chem. **159**, 147–153 (2019). https://doi.org/10.1016/j.radphyschem.2019.02.054

27. J. Zu, M. Ye, P. Wang et al., Design of a strong-base anion exchanger and its adsorption and elution behavior for rhenium(VII). RSC Adv. **6**, 18868–18873 (2016). https://doi.org/10.1039/C5RA25313F
28. K.M. Long, G.S. Goff, S.D. Ware et al., Anion exchange resins for the selective separation of technetium from uranium in carbonate solutions. Ind. Eng. Chem. Res. **51**, 10445–10450 (2012). https://doi.org/10.1021/ie300534e
29. A. Majavu, A.S. Ogunlaja, Z.R. Tshentu, Separation of rhodium(III) and iridium(IV) chlorido complexes using polymer microspheres functionalized with quaternary diammonium groups. Sep. Sci. Technol. **52**, 71–80 (2017). https://doi.org/10.1080/01496395.2016.1235051
30. J. Abdi, M. Vossoughi, N.M. Mahmoodi et al., Synthesis of metal-organic framework hybrid nanocomposites based on GO and CNT with high adsorption capacity for dye removal. Chem. Eng. J. **326**, 1145–1158 (2017). https://doi.org/10.1016/j.cej.2017.06.054
31. M. Hong, L. Yu, Y. Wang et al., Heavy metal adsorption with zeolites: the role of hierarchical pore architecture. Chem. Eng. J. **359**, 363–372 (2019). https://doi.org/10.1016/j.cej.2018.11.087
32. H. Weng, P. Zhang, Z. Guo et al., Efficient and ultrafast adsorption of rhenium by functionalized hierarchically mesoporous silica: a combined strategy of topological construction and chemical modification. ACS Appl. Mater. Interfaces. **13**, 8249–8262 (2021). https://doi.org/10.1021/acsami.0c19290
33. J.P. Stanford, N. van Rooyen, T. Vaidya et al., Photodecomposition of methyl iodide as pretreatment for adsorption of radioiodine species in used nuclear fuel recycling operations. Chem. Eng. J. **400**, 125730 (2020). https://doi.org/10.1016/j.cej.2020.125730
34. M. Thommes, K. Kaneko, A.V. Neimark et al., Physisorption of gases, with special reference to the evaluation of surface area and pore size distribution (IUPAC Technical Report). Pure Appl. Chem. **87**, 1051–1069 (2015). https://doi.org/10.1515/pac-2014-1117
35. L.J. Cao, G. Wang, L. Shi et al., Preparation and catalytic application of poly 4-vinylpyridine microspheres. J. Appl. Polym. Sci. **116**, 3178–3183 (2010). https://doi.org/10.1002/app.31197
36. H. Berk, B. Balci, S. Ertan et al., Functionalized polysulfide copolymers with 4-vinylpyridine via inverse vulcanization. Mater. Today Commun. **19**, 336–341 (2019). https://doi.org/10.1016/j.mtcomm.2019.02.014
37. J. Ortiz-Palacios, J. Cardoso, M. de la Cruz et al., Functionalization in copolymers based on 4VP: DVB for the removal of Cr(VI) ions from aqueous solution. J. Appl. Polym. Sci. **134**, 45548 (2017). https://doi.org/10.1002/app.45548
38. V.A. Pashynska, M.V. Kosevich, A. Gömöry et al., On the stability of the organic dication of the bisquaternary ammonium salt decamethoxinum under liquid secondary ion mass spectrometry. Rapid Commun. Mass Spectrom. **19**, 785–797 (2005). https://doi.org/10.1002/rcm.1846
39. R.R. Srivastava, M.S. Kim, J.C. Lee et al., Liquid–liquid extraction of rhenium(VII) from an acidic chloride solution using Cyanex. Hydrometallurgy. **157**, 33–38 (2015). https://doi.org/10.1016/j.hydromet.2015.07.011
40. T. Kavitha, I.K. Kang, S.Y. Park, Poly(4-vinyl pyridine)-grafted graphene oxide for drug delivery and antimicrobial applications. Polym. Int. **64**, 1660–1666 (2015). https://doi.org/10.1002/pi.4968
41. P. Cyganowski, A. Cierlik, A. Leśniewicz et al., Separation of Re(VII) from Mo(VI) by anion exchange resins synthesized using microwave heat. Hydrometallurgy **185**, 12–22 (2019). https://doi.org/10.1016/j.hydromet.2019.01.013
42. C. Xiong, C. Yao, X. Wu, Adsorption of rhenium(VII) on 4-amino-1,2,4-triazole resin. Hydrometallurgy **90**, 221–226 (2008). https://doi.org/10.1016/j.hydromet.2007.10.011
43. F. Li, Z. Yang, H. Weng et al., High efficient separation of U(VI) and Th(IV) from rare earth elements in strong acidic solution by selective sorption on phenanthroline diamide functionalized graphene oxide. Chem. Eng. J. **332**, 340–350 (2018). https://doi.org/10.1016/j.cej.2017.09.038
44. K.K.H. Choy, D.C.K. Ko, C.W. Cheung et al., Film and intraparticle mass transfer during the adsorption of metal ions onto bone char. J. Colloid Interface Sci. **271**, 284–295 (2004). https://doi.org/10.1016/j.jcis.2003.12.015
45. W.J. Weber Jr., J.C. Morris, Kinetics of adsorption on carbon from solution. J. Sanit. Eng. Div. **89**, 31–59 (1963). https://doi.org/10.1061/JSEDAI.0000430
46. H. Zheng, D. Liu, Y. Zheng et al., Sorption isotherm and kinetic modeling of aniline on Cr-bentonite. J. Hazard. Mater. **167**, 141–147 (2009). https://doi.org/10.1016/j.jhazmat.2008.12.093
47. A. Serva, V. Migliorati, A. Lapi et al., Structural properties of geminal dicationic ionic liquid/water mixtures: a theoretical and experimental insight. PCCP. **18**, 16544–16554 (2016). https://doi.org/10.1039/C6CP01557C
48. M. Shi, Q. Dai, F. Li et al., Membranes with well-defined selective layer regulated by controlled solvent diffusion for high power density flow battery. Adv. Energy Mater. **10**, 2001382 (2020). https://doi.org/10.1002/aenm.202001382
49. Z. Zhang, M.M. Rahman, C. Abetz et al., Quaternization of a polystyrene-block-poly(4-vinylpyridine) isoporous membrane: an approach to tune the pore size and the charge density. Macromol. Rapid Commun. **40**, 1800729 (2019). https://doi.org/10.1002/marc.201800729
50. F.C. Wu, R.L. Tseng, R.S. Juang, Initial behavior of intraparticle diffusion model used in the description of adsorption kinetics. Chem. Eng. J. **153**, 1–8 (2009). https://doi.org/10.1016/j.cej.2009.04.042
51. Status of Contaminated Water Treatment and Tritium at Fukushima Daiichi Nuclear Power Station, Tokyo Electric Power Company, Inc., https://www.meti.go.jp/earthquake/nuclear/pdf/140424/140424_02_008.pdf. Accessed 24 April 2014
52. F.J. Millero, R. Feistel, D.G. Wright et al., The composition of standard seawater and the definition of the reference-composition salinity scale. Deep Sea Res. Part **I**(55), 50–72 (2008). https://doi.org/10.1016/j.dsr.2007.10.001
53. Y. Marcus, Thermodynamics of solvation of ions. Part 5.—Gibbs free energy of hydration at 298.15K. J. Chem. Soc. Faraday Trans. **87**, 2995–2999 (1991). https://doi.org/10.1039/FT9918702995
54. K.W. Kim, Y.J. Baek, K.Y. Lee et al., Treatment of radioactive waste seawater by coagulation–flocculation method using ferric hydroxide and poly acrylamide. J. Nucl. Sci. Technol. **53**, 439–450 (2016). https://doi.org/10.1080/00223131.2015.1055313